Conditional Expression of Human 15-Lipoxygenase-1 in Mouse Prostate Induces Prostatic Intraepithelial Neoplasia: The FLiMP Mouse Model[1]

Uddhav P. Kelavkar, Anil V. Parwani†, Scott B. Shappell‡ and W. David Martin§*

Departments of *Urology and Cancer Institute, and †Pathology and Informatics, University of Pittsburgh, Pittsburgh, PA, USA; ‡Molecular Oncology Diagnostic Laboratory, Dallas, TX, USA; §Department of Pathology, Emory University, Atlanta, GA, USA

Abstract

The incidence and mortality of prostate cancer (PCa) vary greatly in different geographic regions, for which lifestyle factors, such as dietary fat intake, have been implicated. Human 15-lipoxygenase-1 (h15-LO-1), which metabolizes polyunsaturated fatty acids, is a highly regulated, tissue-specific, lipid-peroxidating enzyme that functions in physiological membrane remodeling and in the pathogenesis of atherosclerosis, inflammation, and carcinogenesis. We have shown that aberrant overexpression of 15-LO-1 occurs in human PCa, particularly high-grade PCa, and in high-grade prostatic intraepithelial neoplasia (HGPIN), and that the murine orthologue is increased in SV40-based genetically engineered mouse (GEM) models of PCa, such as LADY and TRansgenic Adenocarcinoma of Mouse Prostate. To further define the role of 15-LO-1 in prostate carcinogenesis, we established a novel GEM model with targeted overexpression of h15-LO-1 in the prostate [human fifteen lipoxygenase-1 in mouse prostate (FLiMP)]. We used a Cre- mediated and a loxP-mediated recombination strategy to target h15-LO-1 specifically to the prostate of C57BL/6 mice. Wild-type (wt), FLiMP$^{+/-}$, and FLiMP$^{+/+}$ mice aged 7 to 21, 24 to 28, and 35 weeks were characterized by histopathology, immunohistochemistry (IHC), and DNA/RNA and enzyme analyses. Compared to wt mice, h15-LO-1 enzyme activity was increased similarly in both homozygous FLiMP$^{+/+}$ and hemizygous FLiMP$^{+/-}$ prostates. Dorsolateral and ventral prostates of FLiMP mice showed focal and progressive epithelial hyperplasia with nuclear atypia, indicative of the definition of mouse prostatic intraepithelial neoplasia (mPIN) according to the National Cancer Institute. These foci showed increased proliferation by Ki-67 IHC. No progression to invasive PCa was noted up to 35 weeks. By IHC, h15-LO-1 expression was limited to luminal epithelial cells, with increased expression in mPIN foci (similar to human HGPIN). In summary, targeted overexpression of *h15-LO-1* (a gene overexpressed in human PCa and HGPIN) to mouse prostate is sufficient to promote epithelial proliferation and mPIN development. These results support 15-LO-1 as having a role in prostate tumor initiation and as an early target for dietary or other prevention strategies. The FLiMP mouse model should also be useful in crosses with other GEM models to further define the combinations of molecular alterations necessary for PCa progression.

Neoplasia (2006) **8,** 510–522

Keywords: Transgenic, mouse model, genetically engineered mouse model, arachidonic acid, prostate cancer

Introduction

Cancer mortality is principally associated with tumor invasion and dissemination. Therefore, understanding the processes by which localized carcinoma evolves into invasive carcinoma will likely have therapeutic implications. In prostate cancer (PCa), disease progression is thought to proceed through multiple steps, from prostatic intraepithelial neoplasia (PIN) to locally invasive carcinoma to metastatic disease. Progression through various stages of tumorigenesis presumably requires alterations in the gene expression of both tumor oncogenes, and tumor-suppressor and mutator genes in initiated cells. Ultimately, these genetic lesions alter cancer cell phenotype by modifying global gene expression patterns.

We demonstrated increased expression of an ω-6 fatty acid linoleic acid (LA)–metabolizing enzyme, 15-lipoxygenase-1 (15-LO-1, ALOX15), in prostate tumor tissues compared with normal adjacent prostate tissues [1,2]. Further work from our laboratory and others [3–8] suggests that the metabolites of polyunsaturated fatty acids directly impact prostate

Abbreviations: FLiMP, fifteen lipoxygenase-1 in mouse prostate; 15-LO-1, 15-lipoxygenase-1; HODE, hydroxyoctadecadienoic acid; LA, linoleic acid; HGPIN, high-grade prostatic intraepithelial neoplasia; GEM, genetically engineered mouse; TRAMP, TRansgenic Adenocarcinoma of Mouse Prostate; CAT, chloramphenicol acetyl-transferase

Address all correspondence to: Uddhav P. Kelavkar, PhD, Urological Research Laboratories, Shadyside Medical Center, Suite G-37, 5200 Center Avenue, Pittsburgh, PA 15232.
E-mail: kelavkarup@upmc.edu

[1]This work was supported by National Institutes of Health grant R21-CA098657-02 (to U.P.K).
Received 27 February 2006; Revised 23 March 2006; Accepted 29 March 2006.

DOI 10.1593/neo.06202

tumorigenesis and that the ability to do so depends on both dietary intake and metabolic enzyme expression [9]. Although arachidonic acid can also act as a substrate for 15-LO-1, yielding the anti-inflammatory and proapoptotic metabolite 15-(*S*)-hydroxyeicosatetraenoic acid, the 15-LO-1 enzyme greatly prefers LA. 15-LO-1 metabolizes LA to 13-(*S*)-hydroxyoctadecadienoic acid [13-(*S*)-HODE], which can regulate cell growth, differentiation, and vascular homeostasis [10–19]. Our data [10–12,20] and other reports [21–24] indicate that 13-(*S*)-HODE is mitogenic and thus enhances cellular proliferation [11,13–19]. Indeed, inhibition of 15-LO-1 enzyme activity causes apoptosis in the PCa cell line PC3 [11,20].

Several of our findings support a possible role for 15-LO-1 in PCa tumorigenesis: 1) expression of 15-LO-1, the gene of which maps to human 17p13.3, was upregulated by a mutant *p53*, but not by a wt p53 [25]; 2) the expression of 15-LO-1 and mutant *p53* correlated with each other and with Gleason grade in prostate tumor epithelium [1]; 3) injection of athymic mice with PC3 cells overexpressing 15-LO-1 resulted in the development of aggressive tumors [11]; 4) expression of 15-LO-1 correlated with the upregulation and activation of the insulin-like growth factor-1 receptor in PCa cells [12]; and 5) analysis of the TARP-2 multitumor human tissue array from the National Cancer Institute (NCI) revealed an increased expression of 15-LO-1 in PCa, lung cancer, breast cancer, melanoma, and colonic adenocarcinoma, compared with normal controls [26]. Recently, we demonstrated that methylation of a single CpG within the second CpG island of an 15-LO-1 promoter is frequently present in individuals with high-grade prostatic intraepithelial neoplasia (HGPIN) and PCa [27]. Our study identified a new role for epigenetic phenomenon in PCa wherein hypermethylation of the 15-LO-1 promoter leads to the upregulation of 15-LO-1 expression and enzyme activity, which contributes to PCa initiation and progression.

Conversely, a decrease in 15-LO-1 activity is observed in colon and esophageal cancers [28–30]. Although many cancers in humans arise from germline mutations occurring in all cells, the majority of cancers in humans arise spontaneously from epigenetic aberrations, such as methylation, that occur in genomic DNA of individual cells. This phenomenon (not genetic mutations) plays am essential role in early PCa development [31]. Therefore, the development of model systems that allow us to mimic this type of spontaneous disease in mice while still maintaining control over the metabolism event is critical to our understanding of the molecular mechanisms leading to chemopreventive recommendations in slowing the progression of human PCa. This is well recognized within the field [Mouse Models of Human Cancer Consortium (MMHCC) members] [32].

To more closely approximate the pattern of the somatic overexpression of 15-LO-1 observed in human prostate neoplasia (PIN) and tumors, we generated transgenic mice using a "flox–stop" approach. This allows for tissue-specific expression of transgene in selected cell types based on the expression pattern of Cre recombinase enzyme in animals. Tissue-specific Cre recombinase activity can be accomplished by breeding to Cre-transgenic mice (as performed here) or by other methods such as viral infection. This latter approach can be used to induce transgene expression in a subset of cells within a given tissue, to better mimic spontaneous human disease [33]. To develop the model, we generated transgenic mice expressing the construct CAG–loxP–CAT–loxP–h15-LO-1 in which 15-LO-1 expression is blocked but chloramphenicol acetyl-transferase (CAT) expression is driven by a ubiquitous CAG promoter. These animals are henceforth called REAGENT mice. These animals were then crossed to transgenic mice that express Cre recombinase under a prostate-specific androgen-responsive probasin (Pb) promoter [34]. This leads to the expression of Cre recombinase in prostate epithelia at puberty, deletion of CAT reporter stop cassette, and subsequent 15-LO-1 expression in all prostatic epithelial cells. The resulting conditional transgenic mouse is called fifteen lipoxygenase-1 in mouse prostate (FLiMP) and expresses human 15-lipoxygenase-1 (h15-LO-1) only in mature prostate. 15-LO-1 expression in these animals predisposes the animals to the development of lesions in an age-dependent fashion that closely resembles human PIN. Our findings confirm that 15-LO-1 has an important role in regulating progression from normal to PIN.

Materials and Methods

Production of CAGloxPCAT–STOPloxPh15-LO-1 (REAGENT) Transgenic Mouse

Plasmid (CAGloxPCAT–STOPloxPh15-LO-1) construction The transgene design is as follows. A strong, constitutive promoter, CAG (consisting of a cytomegalovirus enhancer and a chicken β-actin promoter) [35], is linked to two genetic elements: a *CAT* reporter gene and human 15-LO-1 cDNA. The *CAT* reporter gene lies upstream of 15-LO-1 cDNA and is flanked by two loxP sites, which are recognition sites for the bacterial enzyme Cre recombinase. In the absence of further genetic manipulation, the CAG promoter drives the expression of the *CAT* reporter gene but stop codons at the 3′ end of the reporter, terminating transcription before the initiation of human 15-LO-1 cDNA.

The CAG–loxP–CAT–loxP vector was a kind gift from Dr. Pierre Vassalli (Department of Pathology, University of Geneva, Geneva, Switzerland). The pcDNA3.1 vector containing the 2.7-kb full-length human 15-LO-1 cDNA was excised with *Eco*RI, and the 15-LO-1 cDNA fragment blunt end was cloned by T4 DNA ligase (New England Biolaboratories, Inc., Ipswich, MA) into a predigested CAG vector with *Eco*RV. *Eco*RV digestion removed the cloned *lacZ* gene. This 10-kb CAGloxPCAT–STOPloxPh15-LO-1 construct (Figure 1*A*) was sequence-verified, purified by electrophoresis, eluted with NACS PREPAC (Gibco BRL, Grand Island, NY), and used for microinjection. The plasmid CAGloxPCAT–STOPloxPh15-LO-1 was purified with NACS PREPAC, suspended in 1 mM Tris–HCl (pH 7.5)/0.1 mM EDTA at 5 ng/μl, and used for microinjection. Transgenic mice were produced as described below.

Generation of transgenic mice Transgenic CAGloxPCAT–STOPloxPh15-LO-1 mice (REAGENT) were produced by pronuclear microinjection of day-0.5 embryos from a C57BL/6 strain (NCI Charles River Laboratories, Wilmington, MA) using standard techniques [36]. All potential transgene founders were tailed at 10 to 12 days of age and given a unique identification number using either a toe tattoo or a toe clip system. A microtattooer with a sterile 30-gauge hypodermic needle was used to inject tattoo ink into the toe pads of individual mice for identification with a standard identification chart (Ketchum Manufacturing, Inc., Brockville, Ontario, Canada). Genomic DNA was isolated from the tails of potential founder mice and analyzed for the presence of the CAG–loxP–CAT–loxP–h15-LO-1 transgene using polymerase chain reaction (PCR), with primers located within h15-LO-1 cDNA. The forward primer is located in exon 12 (5′-GTGGAAGGAATCGTGAGTCTCCACT-3′) and the reverse primer is located in exon 14 (5′-GTCTGCCCAGCTGCAGTGATGGA-3′) of the *15-LO-1* gene. The size of the amplified 15-LO-1 transgene is 388 bp, whereas the size of the human genomic 15-LO-1 DNA (used as a positive control) is 1098 bp (Figure 1*B*). The primers do not amplify rat or murine *12/15-LO* gene. The reaction conditions for the PCR were as follows: 95°C/10 minutes, 94°C/30 seconds, 63°C/30 seconds, and 72°C/30 seconds for 35 cycles, with a final extension cycle at 72°C for 5 minutes. PCR products were analyzed by gel electrophoresis and visualized with a BioRad gel capture system (BioRad, Inc., Hercules, CA).

Initial characterization of founder lines Three CAGloxP-CAT–STOPloxPh15-LO-1 (REAGENT) transgenic founder lines were identified, as shown in Figure 2, and designated as lines 1857, 1863, and 1868. All three transgenic founder lines were bred to C57BL/6 wt mice (NCI Charles River Laboratories) and were characterized for germline transmission, tissue tropism, and level of CAT expression. In addition, multiple tissues from all lines were tested for basal h15-LO-1 expression to ensure that there was no aberrant background expression of 15-LO-1. All three lines demonstrated high levels of CAT expression in all tissues tested, without any background expression of h15-LO-1 (Figure 2; data not shown).

CAT assay Transgenic mice from either the three REAGENT lines (1857, 1863, and 1868) or the 1868×Pb-Cre FLiMP line ($n = 4$) were sacrificed at 2 months of age. Tissues were collected and used immediately, or frozen and stored at −80°C. CAT assays were performed as described before [37]. Briefly, each tissue was individually homogenized and heated at 65°C for 8 minutes, and the supernatant was used for CAT and protein determination assays. The concentration of soluble protein was determined by BioRad protein assay. The percentage of [^{14}C]chloramphenicol converted to acetylated forms was determined either by densitometric scanning of autoradiograms using a Phosphorimager (Storm860) with IMAGEQUANT version 5.1 software or by scraping of individual spots from thin-layer chromatography (TLC) and counting in a scintillation counter. CAT activities were expressed as picomoles of acetyl chloramphenicol generated per minute per milligram of protein, after subtracting the background for each tissue from control mice that do not express the *CAT* gene. Specific activity was calculated as picomoles of product per milligram of protein per minute.

Generation and characterization of FLiMP transgenic mouse model The 1868 transgenic line (REAGENT-3) identified above was crossed to Pb-Cre4 mice to generate offspring that carry both transgenes. In Pb-Cre4 mice, Cre expression is prostate-specific, except for a few scattered areas in the gonads and in the stroma of the seminal vesicle. Expression differs between lobes, with expression being highest in the lateral lobe, followed by the ventral lobe, the dorsal lobe, and the anterior lobe, which have lower levels of expression. Resultant pups were PCR-screened for the presence of the CAGloxPCAT–STOPloxPh15-LO-1 transgene, as described above. Mice were also screened for Pb-Cre transgene using a PCR genotyping strategy, as previously described [34]. Male double transgenic mice [hereafter referred to as FLiMP$^{+/+}$ (homozygous) and FLiMP$^{+/-}$ (hemizygous) mice] from the 1868 line were characterized at 8 to 10 weeks of age for the extent of CRE-mediated deletion of the *CAT* reporter gene (by CAT analysis, as described above), and resultant h15-LO-1 expression and activity. FLiMP mice demonstrated efficient deletion of the reporter *CAT* gene and expression of h15-LO-1.

RNA preparation and amplification Sample RNA from dissected dorsal, lateral, anterior, and ventral prostates, each from three transgenic C57BL/6, FLiMP$^{+/-}$, and FLiMP$^{+/+}$ mice at 10, 20, and 30 weeks of age, were pooled and compared to control RNA similarly extracted from age-matched nontransgenic C57BL/6 littermates. Dissected prostate tissues were immediately immersed in RNA*later* (Ambion, Inc., Austin, TX). Total RNA was then purified with DNase I using RNeasy kit (Qiagen, Valencia, CA), following the manufacturer's protocol. RNA was quantified by spectrophotometry (Eppendorf, Hamburg, Germany), and its integrity was assured by analysis using a BioRad Experion RNA analyzer chip (BioRad, Inc.). Real-time quantitative reverse transcription–polymerase chain reaction (qRT-PCR) was performed in a 25-μl mixture containing first-strand cDNA synthesized using 1 μg of total RNA (DNase-treated) and a reverse transcriptase reaction mixture. A 92-bp region of mouse β-actin cDNA using primers 5′-CCTGGCACCCAGCACAAT-3′ and 5′-GCCGATCCACACGGAGTACT-3′ was amplified at 95°C/10 minutes (95°C/30 seconds and 59°C/60 seconds) for 40 cycles using 1× SYBR Green and buffer (PE Applied Biosystems, Foster City, CA), 4 mM $MgCl_2$, 0.2 μM of each primer (β-actin and 15-LO-1), 0.2 mM dNTP mixture, and 0.025 U of AmpliTaq Gold thermostable DNA polymerase (Applied Biosystems, Foster City, CA). A 192-bp region of h15-LO-1 using 15-LO-1 primers 5′-GACCGAGGGTTTCCTGTCTC-3′ and 5′-TGTCTCCAGCGTTGCATCC-3′ was similarly amplified (but without SYBR Green) at 95°C/3 minutes (95°C/30 seconds and 58°C/60 seconds)

for 40 cycles and quantified by a *TaqMan* probe 5′-5HEX-CAGGCTCGGGACCAGGTTTGCCAG-BHQ2a-5HEX-3′. Real-time quantitations were performed using the iQ5 Real-Time PCR Detection System (BioRad, Inc.). Fluorescence threshold was calculated using system software. Optimization experiments showed that PCRs (performed in triplicate) for β-actin were highly reproducible, with a low intra-assay coefficient of variation (0.5%).

Determination of 15-LO-1 expression/activity by enzyme-linked immunosorbent assay (ELISA) To measure 15-LO-1 activity, the level of the LA metabolite 13-HODE in tissues was examined using commercially available ELISA plates (Oxford Biomedical Research, Inc., Oxford, MI). Prostate tissues from transgenic and wt nontransgenic littermate controls were homogenized in 600 μl of buffer containing 50 mM Tris–HCl (pH 7.4), 25 μM LA, and 5 mM $CaCl_2$. In all buffers, protease inhibitors were added just before use: 1 mM phenylmethylsulfonyl fluoride, 1 mM benzamidine, 10 μg/ml aprotinin, 10 μg/ml leupeptin, and 1 μg/ml pepstatin A. After incubation, 0.3 mg of sodium borohydride was added, and the mixture was kept on ice for 15 minutes. This mixture was then acidified with HCl (pH 3.0). The sample was extracted in 2 ml of ethyl ether, the solvent was evaporated, and the dried material was dissolved in 50 μl of methanol/water (3:1) solvent. Concentrations of 13-(*S*)-HODE were represented as micrograms per milliliter per gram of tissue after normalizing for the endogenous 12/15-LO activity of proteins in samples of transgenic wt littermate controls.

Preparation and analyses of tissues for prostate histopathology Individual 1868 $FLiMP^{+/-}$ and $FLiMP^{+/+}$ male mice were sacrificed from 6 to 35 weeks of age and examined for gross organ abnormalities. The urogenital tract was removed intact, and the tissues were dissected to remove the bladder and associated fats. The tissues (including all prostate lobes, and the seminal vesicles) were fixed in buffered formalin. The urogenital tract, including the bladder, seminal vesicles, prostate (dissected dorsolateral, ventral, and anterior lobes), testes, and epididymides, were removed on necropsy en bloc and prepared for pathological evaluation, as described below. For histology, the prostate was treated with an acid alcohol solution, as described by Folkvord et al. [38]. Fixed tissues were embedded in paraffin, and sections were stained with hematoxylin and eosin (H&E) [39]. Prostate lesions were assessed according to the consensus classification of the MMHCC (October 2000; Bar Harbor, ME) by two independent pathologists (A.V.P. and S.B.S.) who were blinded to the genotypes of the animals [32].

Mice were sacrificed at different age time points (as described above), tissues were harvested, and tissue sections were prepared for immunohistochemistry (IHC). The following tissues were analyzed wherever indicated: prostate (anterior, dorsal, lateral, and ventral lobes), regional lymph nodes (lateral iliac and aortic lumbar), liver, lungs, spleen, kidneys, bone (lumbar vertebra), adrenal glands, brain, salivary glands (submandibular and parotid), submandibular lymph nodes, bulbourethral glands, and grossly remarkable skin and subcutaneous tissues. Tissue sections obtained from the mice were deparaffinized and dehydrated, endogenous peroxidase activity was blocked, and sections were treated with normal serum to bind nonspecific sites. The sections were then incubated with primary antibodies or with nonimmune mouse IgG. In this study, rabbit polyclonal anti–Ki-67 antibody was used to study the proliferation index. Secondary IgGs of appropriate species specificity were used. Sections were developed with 3,3-diaminobenzidine (brown). Sections were also counterstained for H&E staining. Control sections were processed in parallel with mouse or rabbit nonimmune IgGs at the same concentration as that with primary antibodies. As generated in this study, polyclonal antibody IgG_1 specific for 15-LO-1—which are h15-LO-1–specific and do not cross-react with either human 5-LO, 12-LO, or 15-LO-2 or with mouse 5-LO, but cross-react minimally with mouse 12/15-LO protein—were used to examine 15-LO-1 protein levels in the tissues. Previously standardized IHC procedures for tissues [1,40] were similarly used in this study.

Results

Generation of FLiMP Mice

To study the consequences of aberrant 15-LO-1 expression on possible prostatic neoplasia development, we used a flox–stop strategy to target human 15-LO-1 expression specifically to the mouse prostate. We generated a targeting vector CAGloxPCAT–STOPloxPh15-LO-1, as shown in Figure 1*A*. In this construct, the CAG promoter drives the expression of the *CAT* reporter gene, but the expression of h15-LO-1 cDNA is blocked due to the poly-A stop signal at the end of the *CAT* gene. Subsequent expression of Cre recombinase in transgenic animals will excise the reporter cassette and allow for the expression of the 15-LO-1 transgene.

Three transgenic founder lines were identified and were named 1857, 1863, and 1868, as shown in Figure 1*B*. All three lines demonstrated germline transmission, and were fertile and viable. The lines were maintained separately on a C57BL/6 background and were tested for the expression of the *CAT* reporter gene in multiple tissues (Figure 2; data for the 1857 and 1863 lines are not shown). All three lines demonstrated high levels of CAT activity in all tissues tested. Mice from each line were also screened for basal h15-LO-1 expression to ensure that there was no leak in the model system. None of the animals tested demonstrated basal 15-LO-1 expression (data not shown). The 1868 line was chosen for future experiments and bred to Pb-Cre mice to generate the FLiMP model. All subsequent experimental data were produced with this line.

Mice for line 1868 were bred to Pb-Cre mice and tested for reporter cassette deletion and h15-LO-1 expression. At 8 weeks, the mice became sexually active and their prostates matured. As expected, Cre-mediated recombination on week 8 resulted in the deletion of the CAT cassette specifically in the prostate, whereas CAT activity remained identical to the founder line in all other tissues tested (Figure 2, *A versus B and C*). These animals are hereafter referred to

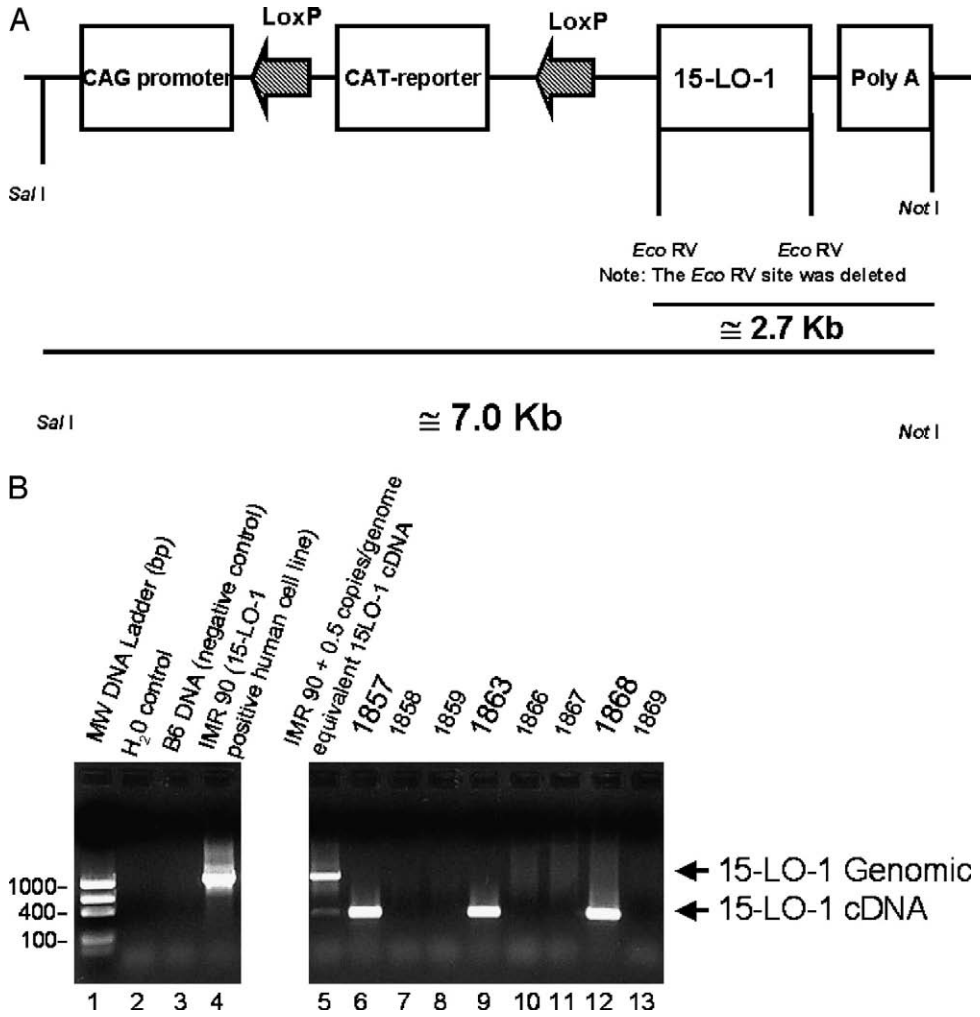

Figure 1. *(A) Map of the pCAG–loxP–CAT–loxP–h15-LO-1 construct. (B) Screening for h15-LO-1 transgenic mouse founders. Lane 1: M_W DNA ladder. Lane 2: H_2O control. Lane 3: B6 DNA (negative control). Lane 4: IMR 90 (human cell line). Lane 5: IMR 90 spiked with 0.5 copies/genome, equivalent to h15-LO-1 cDNA. Lane 6: 1857. Lane 7: 1858. Lane 8: 1859. Lane 9: 1863. Lane 10: 1866. Lane 11: 1867. Lane 12: 1868. Lane 13: 1869. The size of the transgene band is 388 bp, whereas the size of the human genomic DNA (used as positive control) is 1098 bp.*

as FLiMP and are studied in three age ranges: 7 to 10, 18 to 21, and 28 to 35 weeks. FLiMP$^{+/-}$ mice from these matings were further interbred to obtain homozygous (FLiMP$^{+/+}$) animals. In this study, we have examined these mice for prostate phenotypic changes up to 35 weeks (i.e., 8 months) of age starting on week 7 or week 8.

Expression Patterns of h15-LO-1 in FLiMP Mice

Using qRT-PCR and ELISA (for enzyme activity), we confirmed the expression of h15-LO-1 mRNA and enzyme activity in the different prostate lobes of FLiMP mice. Human 15-LO-1 was detected in the prostates of FLiMP$^{+/+}$ and FLiMP$^{+/-}$, but neither in wt (control) mice nor in the parental REAGENT line that was not crossed to Pb-Cre. Although the levels of h15-LO-1 mRNA were approximately twice in FLiMP$^{+/+}$ *versus* FLiMP$^{+/-}$ (Figure 3, *B* and *C*), 15-LO-1 enzyme activity was not significantly different in the individual prostate lobes examined and remained constant at 8, 14, 21, and 3 weeks of age (data not shown). 15-LO-1 activity in different regions of the prostate from FLiMP$^{+/+}$ and FLiMP$^{+/-}$ was normalized for endogenous 12/15-LO (murine orthologue) activity with age-matched nontransgenic littermates. The 15-LO-1 activities assessed by 13-(*S*)-HODE formation were also found to be similar in FLiMP$^{+/+}$ *versus* FLiMP$^{+/-}$ (Figure 4).

Relative expression levels of 15-LO-1 mRNA in FLiMP prostate lobes were in the following order: lateral > ventral > dorsal > anterior lobe of the prostate (Figure 3). By contrast, none of the other tissues examined, including the bladder, brain, bulbourethral gland, heart, kidneys, large intestine, small intestine, liver, lungs, seminal vesicles, spleen, stomach, and testes, showed detectable h15-LO-1 mRNA (data not shown).

Because transgene expression driven by Pb-Cre is expected to be restricted to luminal epithelial cells of the prostate in transgenic mice, it was important to determine the cell type–specific expression pattern of 15-LO-1 in FLiMP prostates as well. By IHC, we found that, in adult

FLiMP mouse prostates, h15-LO-1 expression was restricted to luminal epithelial cells (similar to that in human prostate) and had no detectable immunostaining in either basal cells or in the stromal compartment (Figure 5, *A* and *B*). Histopathological alterations in FLiMP mice were correlated with h15-LO-1 expression by IHC. Although cells in hyperplastic foci consistently expressed normal levels of mouse 12/15-LO, many cells in the foci that were compatible with mouse prostatic intraepithelial neoplasia (mPIN) displayed h15-LO-1 protein expression that was higher than those in histologically normal areas in FLiMP mice and in prostates of wt mice. All such mPIN foci showed such increased h15-LO-1 immunostaining. These foci also showed increased labeling of Ki-67 with age (Figure 5, *C versus D*). Hence, proliferative foci histologically indicative of mPIN were those focally expressing h15-LO-1, strongly supporting a causative role for this gene in the mPIN phenotype observed.

Histopathology and IHC Characterization of FLiMP Mice: Age-Dependent Progressive Prostatic Epithelial Hyperplasia with Atypia Indicative of mPIN

Blinded histopathology analyses of dorsal prostate (DP) and lateral prostate (LP) sections of both FLiMP$^{+/+}$ and FLiMP$^{+/-}$ mice compared to age-matched wt littermate control mice demonstrated focal epithelial stratification with generally mild nuclear atypia. In examined mice, such lesions were observed at increasing frequency with age, and both their extent and architectural abnormalities were also noted to progress with age in FLiMP mice, satisfying the NCI MMHCC criteria for mPIN (Figures 6 and 7; Table 1).

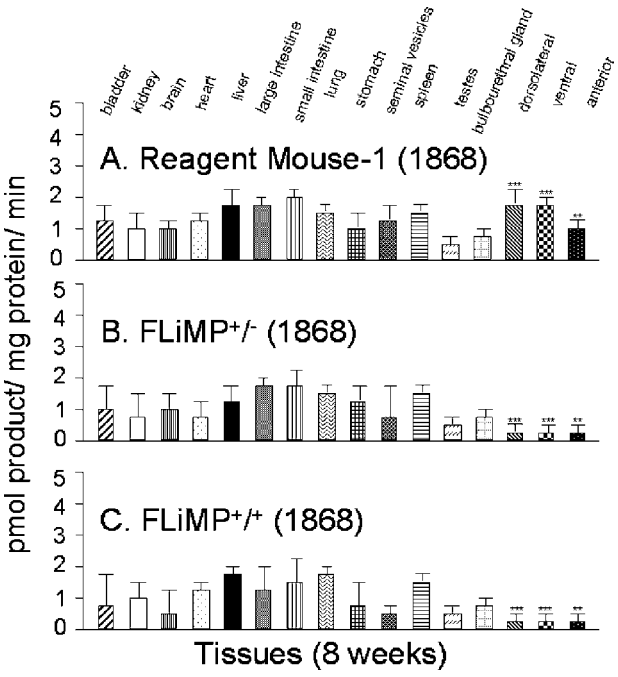

Figure 2. *CAT screening of tissues from REAGENT transgenic male founder, and FLiMP$^{+/-}$ and FLiMP$^{+/-}$ transgenic mice at the 8-week time point (n = 4 each). Tissues were collected and used immediately, or frozen and stored at −80°C. Each tissue was individually homogenized and heated, and the supernatant was used for CAT and protein determination assays. The concentration of soluble protein was determined by BioRad protein assay. The percentage of [^{14}C]chloramphenicol converted to acetylated forms was determined by scraping individual spots with TLC and by counting in a scintillation counter. CAT activities are expressed as picomoles of acetyl chloramphenicol generated per minute per milligram of protein, after subtracting the background for each tissue from control mice that do not express the CAT gene. Specific activity was calculated as picomoles of product per milligram of protein per minute. ***P < .01; **P < .05.*

As noted in Table 1, one of the wt animals showed very focal and mild proliferation and very minimal atypia on blinded review, which was barely, if at all, discernible from normal on retrospective review. There was no increase in frequency of proliferation in wild types, compared to that documented in FLiMP$^{+/-}$ and FLiMP$^{+/+}$ mice (Table 1). In contrast, the percentage of older animals with histopathological evidence of proliferation with atypia in FLiMP$^{+/-}$ and FLiMP$^{+/+}$ mice ranged from 10% to 60% (Table 1). Strikingly, these changes were progressive, as evidenced by an increase in the percentage of FLiMP$^{+/-}$ and FLiMP$^{+/+}$ mice with proliferation and atypia in the dorsal and lateral lobes of the prostate (50–60%) (Table 1).

In the DP, tufting and micropapillary patterns of epithelial stratification with atypia, corresponding to the most common architectural patterns of human HGPIN, were noted [32]. In the proximal DP, tufting foci were noted to be difficult to distinguish from the prostate of wt mice, which have slightly greater tufting and architectural complexity in the proximal ducts, closest to the urethra (Figure 6). However, particularly with increasing age, micropapillary projections of mildly atypical epithelium were also noted in distal gland lumens—a morphology quite distinct from the typically flat cuboidal epithelial lining of wt DP, which has minimal focal tufting. The nuclei showed mild enlargement, including elongation and hyperchromasia (Figure 6). No foci suspicious for invasive carcinoma were noted in any section of FLiMP$^{+/-}$ or FLiMP$^{+/+}$ mice examined, and there were no changes noted in the stroma of FLiMP mice compared to wt prostates (Figure 6).

Histopathological alterations in the LP were even more prominent, possibly related to the higher level of h15-LO-1 transgene expression achieved. Compared to the rather simple flat epithelium in wt LP, FLiMP LP sections showed progressively severe nuclear stratification, even achieving focal cribriform architecture (Figure 7). Nuclear atypia was evident (with some enlargement and hyperchromasia) with chromatin clumping. The atypia was milder than that seen in SV40-based models, such as LADY and TRansgenic Adenocarcinoma of Mouse Prostate (TRAMP), and was more in keeping with degrees seen in other mPIN-containing non–SV40-based genetically engineered mouse (GEM) models [32] and human HGPIN.

In some such foci, small nests and microacinar formations were evident beneath the tufting epithelium, in a possibly thickened surrounding fibromuscular stroma. In some models that progress to unequivocally more extensive invasive carcinoma, such lesions have been regarded as microinvasive carcinoma—a classification within the MMHCC Pathology Classification [32]. However, in the sections examined, no such unequivocal foci of invasion into the surrounding looser connective tissues, of an extent indicative of the classification of invasive carcinoma, were noted. Hence,

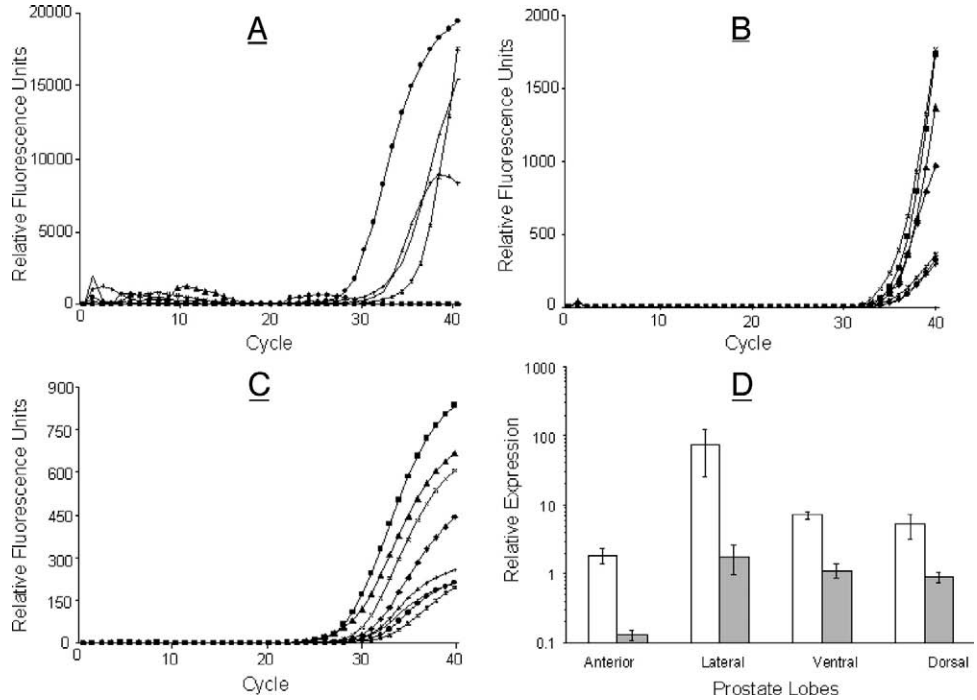

Figure 3. *Real-time qRT-PCR screening. Extracted RNA were quantitated for mouse β-actin and h15-LO-1 from dissected prostate lobes of wt age-matched C57BL/6 littermate controls (A) compared to hemizygous (B) and homozygous (C) FLiMP mice. RNA from dissected dorsolateral, anterior, and ventral prostate lobes, each from three transgenic C57BL/6 FLiMP$^{+/-}$ (hemizygous) and FLiMP$^{+/+}$ (homozygous) mice at 10 weeks of age, were compared to control RNA similarly extracted from wt mice. Real-time quantitations were performed using the iQ5 Real-Time PCR Detection System, as described in the Materials and Methods section. A comparative relative expression level of h15-LO-1 mRNA in different prostate lobes of homozygous (□) and hemizygous (▤) mice is represented (D). Fluorescence threshold values were calculated using the system software. (♦) 15-LO-1 anterior; (■) 15-LO-1 lateral; (▲) 15-LO-1 ventral; (×) 15-LO-1 dorsal; (*) β-actin anterior; (●) β-actin lateral; (+) β-actin ventral; (–) β-actin dorsal.*

the significance of such potentially microinvasive foci in FLiMP LP remains to be further elucidated. In addition, in one LP section of a 35-week-old FLiMP$^{+/+}$ mouse, a focus histologically compatible with perineural invasion (PNI) was noted (Figure 7). In the human prostate, properly defined PNI is considered pathognomonic for invasive prostate carcinoma. Similarly, in GEM prostate pathology, PNI is thought to have similar significance when observed in the setting of models that have demonstrated progression to unequivocal invasive prostate carcinoma [32]. Hence, at present, the significance of this observation in one FLiMP LP remains to be more fully elucidated.

No significant histopathological alteration was noted in the AP of FLiMP$^{+/+}$ or FLiMP$^{+/-}$ mice up to 35 weeks, perhaps consistent with the low level of h15-LO-1 expression noted in the AP. The VPs were not systematically analyzed in the current study, but foci of pathology similar to that in the LP or the DP were not noted in the sections examined. The periurethal glands were extensively sampled in FLiMP mice (present in the majority of animals examined), and no lesions analogous to hyperplasias, atypical hyperplasias, or carcinomas observed in other GEM models [32] were noted in any of the examined animals up to 35 weeks. Likewise, with equally extensive sampling of the related male accessory tissues of the ampullary glands and seminal vesicles, no lesions were noted in FLiMP mice up to 35 weeks (data not shown).

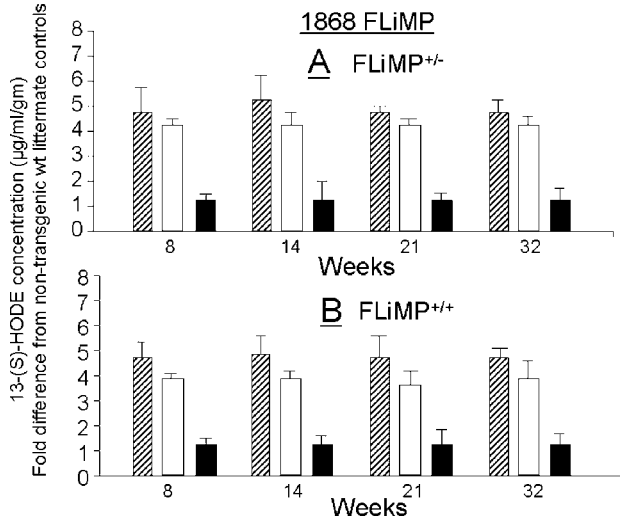

Figure 4. *13-HODE levels in tissues, as a measure of 15-LO-1 activity, were examined using commercially available ELISA plates, as described in Materials and Methods section. Concentrations of 13-(S)-HODE were represented as micrograms per milliliter per gram of tissue after normalizing for the endogenous murine 12/15-LO protein similarly extracted from transgenic wt littermate control samples. Proteins extracted from dissected dorsolateral (▨), ventral (□), and anterior (■) prostate lobes, each from three transgenic C57BL/6, FLiMP$^{+/-}$ (A), and FLiMP$^{+/+}$ (B) mice at 8, 14, 21, and 32 weeks of age, were compared to age-matched nontransgenic C57BL/6 littermate wt control proteins that were similarly extracted and pooled.*

Discussion

GEM models of PCa have been developed by either introducing SV40 T-antigen or knocking out tumor-suppressor genes [32,41]. A GEM model of a disease represents a vital way by which to study both the pathobiology and the effect of new therapeutic strategies. Validation criteria include a comparison of histopathological, genetic, biochemical, and natural history features of the GEM model with known aspects of human PCa, including relevant changes at different stages of progression of this complex and heterogeneous neoplasm [32,42–44]. Animal models can provide an essential resource for testing the efficacy of potential chemopreventive agents [45]. Historically, xenograft models, which use injection or implantation of established tumor cell lines into immunodeficient host mice, have been widely used for chemoprevention studies. Although these models offer many advantages, including ease of experimental manipulation and short time frame for analyses, there are several notable drawbacks to their use for chemoprevention studies. Firstly, the cell lines used for xenografts are typically highly transformed and have been selected for growth in cell culture, which obviously does not recapitulate the natural progression of cancer, particularly in the early stages of the disease. Secondly, the use of immunodeficient mice eliminates an intact host immune response, which is likely to play an important role in prostate carcinogenesis [46].

Precise molecular events associated with the initiation of prostate carcinoma are unknown. PIN is widely regarded as a precursor of human PCa [47,48]. Our results have identified a new and important role for 15-LO-1 in the initiation

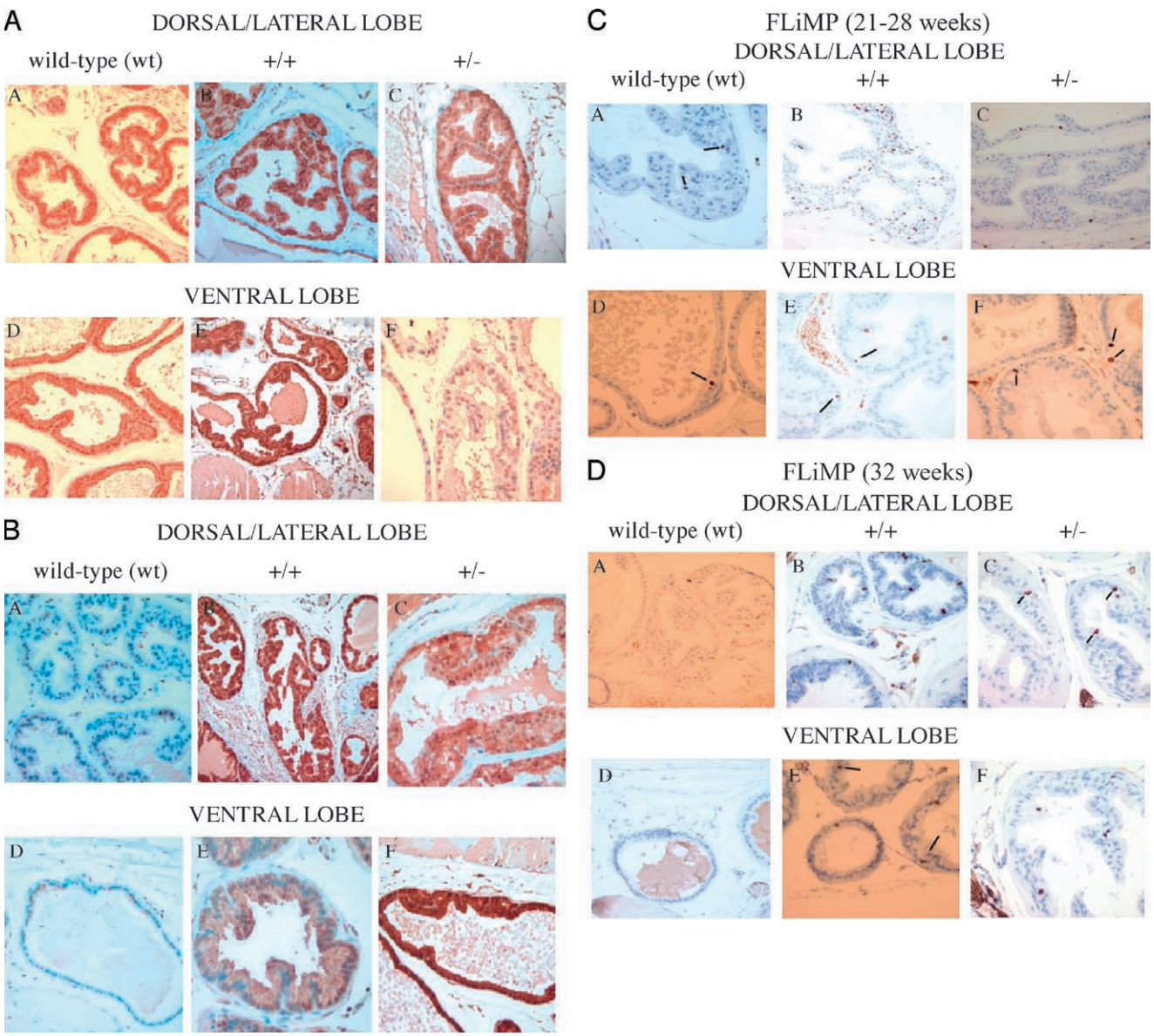

Figure 5. *Representative immunostaining of dorsolateral prostate (DLP) and ventral prostate lobes from homozygous (B and E) and hemizygous (C and F) FLiMP mice compared to wt littermate controls (A and D) at 28 weeks (A) and 35 weeks (B) with polyclonal antibody for h15-LO-1 (original magnification, ×100). Similarly, representative immunostaining of the same mice, as described above at 28 weeks (C) and 35 weeks (D), with polyclonal antibody for Ki-67 (original magnification, ×100) is shown by arrows.*

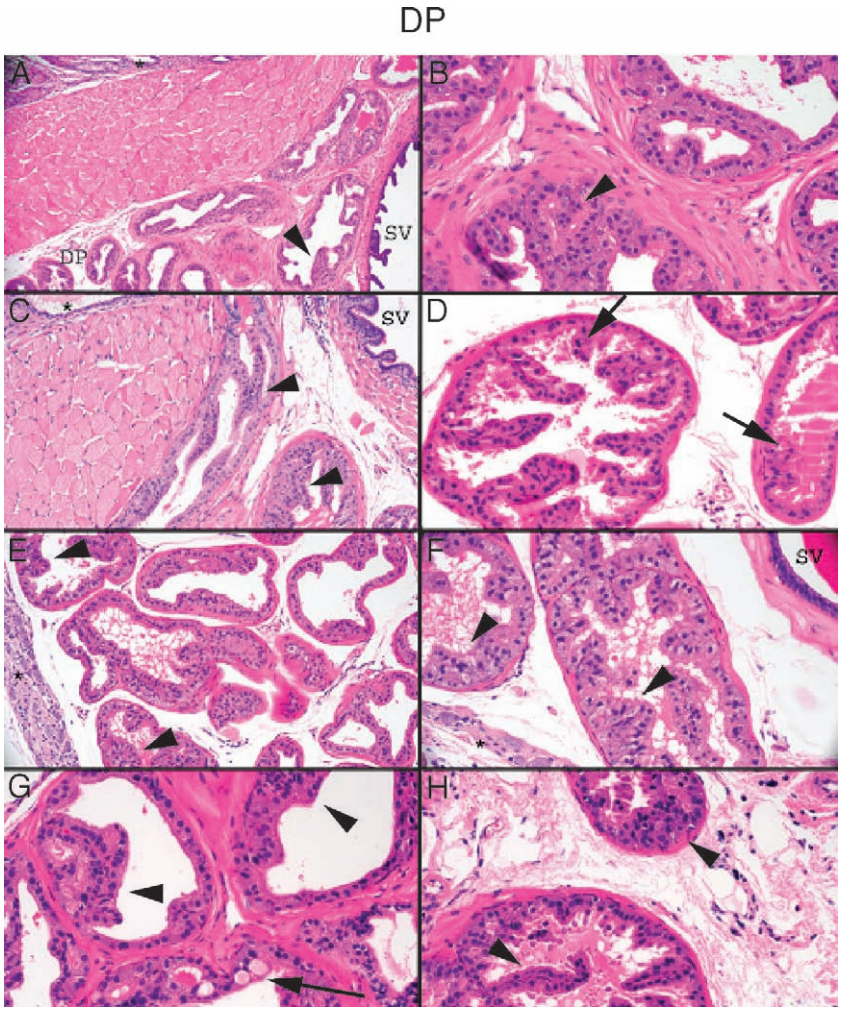

Figure 6. *Representative histopathology of dorsal prostate (DP) sections of FLiMP mice. (A) Intermediate magnification of a 14-week-old FLiMP$^{+/-}$ mouse showing focal epithelial stratification and small cribriform architecture within a normal-sized proximal duct lumen (arrowhead). Urethra/periurethral ducts on the top left (*). Seminal vesicle lumen on the bottom right (SV). More distal DP portions, with a usually thin rim of fibromuscular stroma surrounding individual gland lumens, are shown on the left (DP). (B) Higher magnification of the same 14-week-old FLiMP$^{+/-}$ mouse, showing mild epithelial stratification with minimal nuclear atypia in proximal DP lumen, with focal mitotic figures (arrowhead). (C) Proximal DP area of wt mouse. Urethral lumen on the top left (*). Seminal vesicle on the top right (SV). Normal proximal duct lumens can have more epithelial stratification and architectural complexity (arrowheads) than more distal DP lumens, making the distinction of pathological epithelial proliferations without prominent atypia in these locations difficult to distinguish from the normal wt prostate histologic spectrum. (D) Focal epithelial proliferation with minimal to mild atypia in distal DP portions of a 28-week-old FLiMP$^{+/-}$ mouse. Tufting and micropapillary architecture greater than the usual limited tufting of wt DP are evident, architecturally similar to those that are common in human PIN. Scattered apoptotic bodies were noted (arrows). (E) Intermediate magnification of DP in a 28-week-old FLiMP$^{+/+}$ mouse showing focal epithelial stratification with tufting in multiple lumens (arrowheads). A ganglion (typical of loose stroma surrounding the DLP) is noted on the left (*). (F) Higher magnification of the DP of the same 28-week-old FLiMP$^{+/+}$ mouse as in (E). Epithelial proliferation, manifested as stratification and tufting, with mild atypia is noted in multiple foci (arrowheads). The architecture is quite distinct from the cuboidal epithelium, with minimal focal tufting in wt DP. (G) Proximal DP of a 35-week-old FLiMP$^{+/+}$ mouse showing epithelial tufting, with mild atypia, in multiple lumens (arrowheads). An adjacent lumen shows focal microacinar spaces or signet ring–like cells within the luminal epithelium or the signet ring (arrow). (H) Distal DP of the same 35-week-old FLiMP$^{+/+}$ mouse showing tufting and micropapillary epithelial stratification with mild atypia. The focality and progression (in extent) of such epithelial proliferations with some nuclear atypia are compatible with definitions of mPIN (H&E staining). (B, D, F, G, H) Original magnification, ×400. (A, C, E) Original magnification, ×200.*

of PCa. Previous studies using well-characterized mouse models of PCa support a role for 15-LO-1 in cancer pathobiology [40,49]. We observed a robust expression of the murine orthologue of human 15-LO-1 (12/15-LO) in samples of both HGPIN and lung metastasis from TRAMP mice [40]. This observation also holds true for the large Pb T antigen transgenic PCa mouse model [49]. Therefore, we felt that it was logical to extend these results by independently analyzing the effect of the overexpression of 15-LO-1 on a novel transgenic system. Our present study, characterizing the FLiMP transgenic mouse model, has confirmed that it demonstrates a phenotype that is consistent with human HGPIN, and a close association between aging and progression to neoplasia. As 15-LO-1 also plays an essential role in the development and differentiation of the prostatic epithelium, it provides an important link between development and carcinogenesis in the prostate gland. Several groups have previously reported another gene, called *Nkx3.1*, that plays a role in the development of PIN as a tumor-suppressor gene [50–54]. This was demonstrated by conventional gene

knockout techniques using Nkx3.1–deficient mice. Similar to our study with FLiMP, Nkx3.1 knockout animals also developed prostatic epithelial neoplasia in the setting of developmental abnormalities of the prostate. However, FLiMP mice display mPIN-like lesions after 5 months, compared to Nkx3.1 knockout mice that develop mPIN only after 1 year.

The lesions that developed in FLiMP mice resemble human PIN in several respects. In addition to histopathological similarities, the lesions showed a similar pattern of Ki-67 expression and partial disruption of basal cells, as seen with human PIN lesions. Thus, conditional expression of 15-LO-1 in adult mice predicted the consequences in the

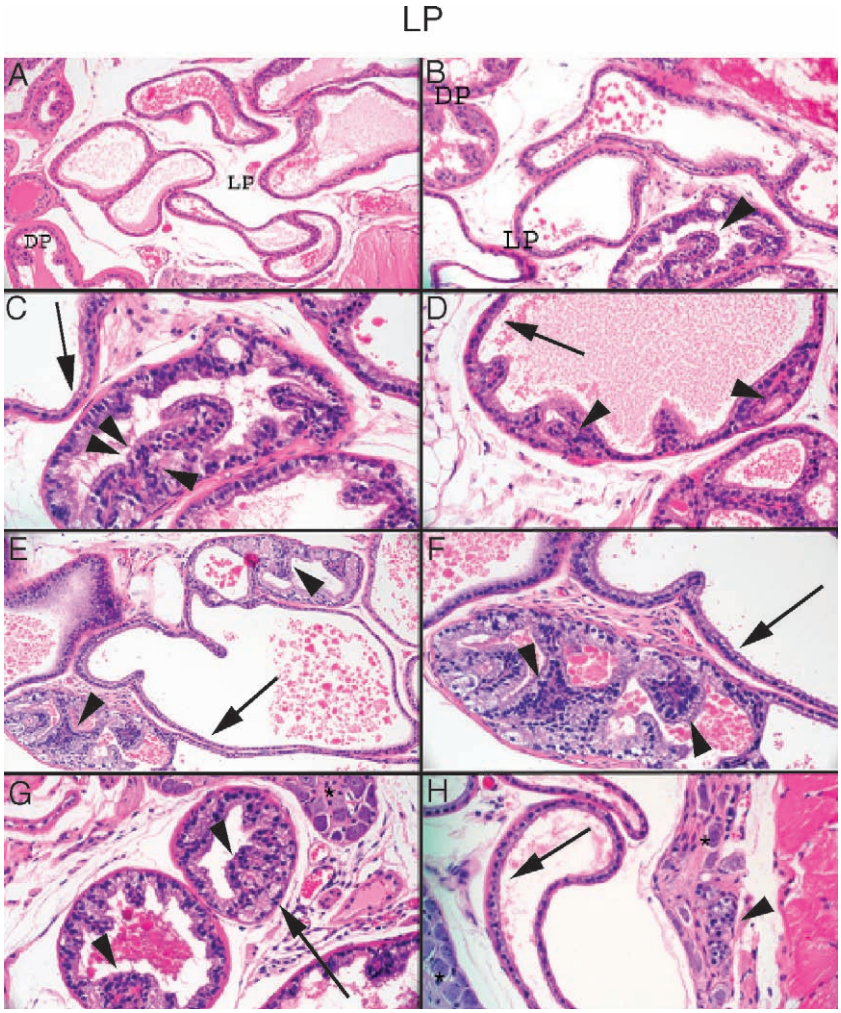

Figure 7. *Histopathology of the lateral prostate (LP) of FLiMP Mice. (A) Intermediate magnification showing normal LP (right) and DP (left). wt LP contains duct lumens with simple cuboidal to columnar epithelium, with basilar nuclei and typically clear to lightly granular eosinophilic cytoplasm. There is usually no tufting to minimal tufting, such that the luminal epithelial lining is flat or smooth. A thin rim of fibromuscular stroma surrounds the epithelium. A ganglion is noted in mid-bottom, in the loose surrounding stroma. (B) The LP of a 28-week-old FLiMP$^{+/-}$ mouse showing focal epithelial proliferation, involving a single gland profile at the bottom center (arrowhead). Residual normal-appearing LP gland lumens are present (LP, center), and a portion of DP is shown on the top left. (C) Higher magnification of a 28-week-old FLiMP$^{+/-}$ mouse LP is shown in (B). The gland lumen shown is extensively involved with epithelial proliferation, with cell stratification seen in areas with tufting and micropapillary architecture (arrowheads). Intraluminal micropapillary proliferation appears to contain a central core of vascularized fibromuscular stroma. There is mild nuclear atypia, with nuclear enlargement/elongation and hyperchromasia. An area of epithelium within the fibromuscular stroma of this particular gland profile (right-hand side, about 4 o'clock) was interpreted as due to tangential sectioning and is not indicative of invasion. The focality of the lesion is evident by comparison to residual normal-appearing LP gland profiles (arrow, top left). (D) The LP of a 28-week-old FLiMP$^{+/+}$ mouse, showing areas of tufting of the epithelium into the gland lumen (arrowheads). In some such foci (as illustrated in focus at the right arrowhead), there were microacinar spaces within the fibromuscular stroma under areas of the tufting epithelium. In some GEM models, these types of lesions have been classified as microinvasive carcinoma. The significance of these foci in the FLiMP model remains to be further characterized, as more unequivocal areas of invasive carcinoma, including extension through fibromuscular stroma into surrounding loose connective tissues, have not been noted. (E) Intermediate magnification of the LP of a different 28-week-old FLiMP$^{+/+}$ mouse showing two gland profiles that are prominently involved in epithelial proliferation with mild atypia (arrowheads). Residual more-normal-appearing LP glands are also evident (arrow, center). (F) Higher magnification of one LP region shown in (E), from a 28-week-old FLiMP$^{+/+}$ mouse. Epithelial proliferation takes the form of micropapillary luminal projections and even cribriform architecture (arrowheads). There are nuclear stratification and mild nuclear atypia, with enlargement/elongation and hyperchromasia. (G) The LP of a 35-week-old FLiMP$^{+/+}$ mouse showing two adjacent gland profiles with epithelial proliferation with atypia, manifested as prominent stratification and tufting into the gland lumens (arrowheads). On focus on the top right, the area of epithelial tufting is accompanied by single cells, small nests, and microacini of similar cells within a thickened fibromuscular stroma (thin strips of stroma that are evident between luminal facing cells and underlying nests), strongly raising the consideration of microinvasion (arrow). Areas of more unequivocal invasion into surrounding looser stroma were not noted. A ganglion is noted on top (*), typical of the DLP. The presence of progressively more prominent atypical epithelial proliferation (e.g., compare lesions in G versus D) is diagnostic of mPIN, according to a standardized NCI GEM prostate pathology classification scheme. (H) The LP of a different 35-week-old FLiMP$^{+/+}$ mouse, showing a focus suspicious for PNI (arrowhead), with nests of epithelium within the nerve/ganglion (*).*

Table 1. Histochemistry and Pathological Description in Prostates of Aging FLiMP and wt Littermate Control Mice.

Mice	Lobe	7–21 weeks		24–28 weeks		35 weeks	
		Histology* (*n*)	Proliferation with Atypia† [*n* (%)]	Histology* (*n*)	Proliferation with Atypia† [*n* (%)]	Histology* (*n*)	Proliferation with Atypia† [*n* (%)]
wt	DP	10	1‡ (10)	2	0	6	0 (0)
	LP	9	1‡ (10)	2	0	6	0 (0)
+/–	DP	8	2 (25)	10	3 (30)	2	1 (50)
	LP	9	1 (11)	9	3 (25)	2	1 (50)
+/+	DP	7	1 (14)	9	5 (55)	9	5 (56)
	LP	7	1 (14)	8	3 (38)	5	3 (60)

*Number of mice for which extensive sections of individual indicated lobes were present for blinded histologic review.
†Number/percent of mice with any degree of focal proliferation and any degree of nuclear atypia. The objective of the table is to document an increase in the number/percent of mice with proliferation and atypia. The numbers do not take into account the severity of these changes (i.e., extent of abnormalities within given mice, degree of proliferation within foci, and severity of nuclear atypia). The increase in the severity of the lesions with time is documented in the text and in the figures.
‡Very focal and mild proliferation and very minimal atypia on blinded review, which are barely, if at all, discernible from normal on retrospective review; no increase in the frequency of proliferation was noted in wt mice *versus* FLiMP$^{+/-}$ and FLiMP$^{+/+}$ mice. Lesions, as noted in 24- to 35-week-old FLiMP mice and as described in the text and in Figures 6 and 7, were not seen in wt mice.

initiation of PCa in humans. All of the FLiMP$^{+/-}$ and FLiMP$^{+/+}$ mice that we studied developed focal epithelial hyperplasia. In a subset of these animals, PIN-like lesions were also observed, and these PIN lesions showed high 15-LO-1 expression, as determined by IHC. The precise mechanism of an aberrant overexpression of 15-LO-1 in PIN and PCa is presently unclear, but may involve epigenetic mechanisms such as promoter hypermethylation [27], leading to overexpression of 15-LO-1. This is particularly intriguing, as studies have independently suggested a positive correlation between high–ω-6 fat diets [55–57] and methylation in human prostate tumors [47,58].

We have shown that, in both mature human and mouse prostates, 15-LO-1 expression is limited to the luminal epithelial cell layer. Our results suggest that aberrant expression of 15-LO-1 in luminal cells is permissive of dedifferentiation and reentry into the cell cycle, subsequently leading to the development of PIN. The mechanism by which the 15-LO-1 and LA metabolic product 13-HODE engages the cell cycle machinery in prostate cells in different developmental stages of the prostate gland and in carcinoma is an interesting subject that warrants further investigation. Additional unanswered questions include whether PIN lesions in conditional FLiMP transgenic mice can progress to invasive carcinoma and metastases with aging or by other hormonal, dietary, or genetic manipulations. Further studies, which include variables such as aging for longer periods, and high ω-6 fatty acid dietary studies are in progress to address this question. Therefore, the FLiMP mouse model provides a novel model system for studying the PIN stage of PCa development because it recapitulates a much earlier PIN phenotype than that observed in NKX3.1 conditional knockout mice.

Transgenic mice can provide valuable models for chemoprevention studies. However, it was only recently that the community of PCa researchers began to accept the idea of using transgenic and mutant mice to study human PCa. In previous years, there has been a great deal of skepticism regarding the relevance of such models, based on significant anatomic and histologic differences between the mouse prostate and the human prostate, and the low incidence of spontaneous PCa in mice (discussed in Abate-Shen and Shen [59,60]). However, it is becoming increasingly clear that the molecular mechanisms underlying PCa progression are highly conserved between mice and humans [50,60–62]. "First-generation" mouse models of PCa, which were pioneered by Greenberg, Matusik, and others, were based on the expression of SV40 oncogenes on the prostatic epithelium under the control of promoters that display prostate specificity, such as that for the Pb gene (reviewed in Wu et al. [34] and Huss et al. [61]). These transgenic mice, particularly the well-studied TRAMP and LADY models, undergo a series of progressive changes from PIN to invasive cancer and metastases with relatively short latency (2–6 months) and have been valuable for molecular analyses of prostate carcinogenesis. In addition, these models have been used for chemoprevention studies to test the efficacy of certain dietary and pharmaceutical agents [63–65]. We have taken a complementary approach by generating a "second-generation" FLiMP transgenic mouse model by overexpressing the human 15-LO-1 enzyme, which is known to be relevant for human PCa. Some other relevant second-generation transgenic and mutant mice include Nkx3.1, Pten, and p27kip1 [34,51–53, 66–70]. Importantly, histopathological and molecular analyses of these mutant mice and our transgenic FLiMP mice have validated their similarity to human PCa.

It is conceivable that 15-LO-1 enzyme activity, in concordance with the acquisition of Nkx3.1 mutation, could be sufficient to drive prostate epithelial transformation (i.e., PIN progression to PCa *in vivo*). An advantage to this system, which we feel is particularly relevant for PCa, is that the double transgenic (compound) model can mimic two naturally occurring early events in PCa development that otherwise are individually insufficient to cause progression to carcinoma. Thus, 15-LO-1 is clearly necessary but not sufficient in itself to cause PCa, supporting the multihit hypothesis. A study with FLiMP$^{+/+}$, Nkx3.1$^{-/-}$ compound mouse model will provide relevant insights for PCa progression, especially initiation events leading to PCa. Therefore, the

FLiMP mouse model is likely to provide extensive data on early events correlating to PIN that are essential for PCa initiation and for the development of a therapeutic model for an effective early treatment of PCa.

To our knowledge, this is the first study to use a transgenic mouse model (FLiMP) to demonstrate a role of h15-LO-1 in the development of prostate lesions that resemble mPIN. Thus, 15-LO-1 has an important role in regulating progression from normal to PIN. The use of the FLiMP mouse model will assist investigators in gaining better understanding, particularly regarding the cooperative effects of multiple genes on PCa initiation and cancer predisposition, as 15-LO-1 expression and function may not be sufficient to cause PCa in mice at 5 months of age.

Acknowledgements

We thank Tom Eling National Institute of Environmental Health Services for the CAG construct. We also thank Justin Hutzley for excellent technical assistance, and Malabika Sen, Teresa Quackenbush, and Lauren Hayes for necropsy and dissection of the different regions of the mouse prostate glands. We thank Rajiv Dhir for preliminary screening of pathology slides, and Moira Hitchens for critical reading and editing of the manuscript.

References

[1] Kelavkar UP, Cohen C, Kamitani H, Eling TE, and Badr KF (2000). Concordant induction of 15-lipoxygenase-1 and mutant *p53* expression in human prostate adenocarcinoma: correlation with Gleason staging. *Carcinogenesis* **21,** 1777–1787.

[2] Kelavkar U, Lin Y, Landsittel D, Chandran U, and Dhir R (2006). The Yin and Yang of 15-lipoxygenase-1 and Delta-5-desaturase: dietary omega-6 linoleic acid metabolic pathway in prostate carcinogenesis. *J Carcinog* **5,** 9.

[3] Liu B, Khan WA, Hannun YA, Timar J, Taylor JD, Lundy S, Butovich I, and Honn KV (1995). 12(*S*)-hydroxyeicosatetraenoic acid and 13(*S*)-hydroxyoctadecadienoic acid regulation of protein kinase C-alpha in melanoma cells: role of receptor-mediated hydrolysis of inositol phospholipids. *Proc Natl Acad Sci USA* **92,** 9323–9327.

[4] Honn KV, Tang DG, Grossi I, Duniec ZM, Timar J, Renaud C, Leithauser M, Blair I, Johnson CR, Diglio CA, et al. (1994). Tumor cell–derived 12(*S*)-hydroxyeicosatetraenoic acid induces microvascular endothelial cell retraction. *Cancer Res* **54,** 565–574.

[5] Tang DG and Honn KV (1994). 12-Lipoxygenase, 12(*S*)-HETE, and cancer metastasis. *Ann NY Acad Sci* **744,** 199–215.

[6] Chen YQ, Duniec ZM, Liu B, Hagmann W, Gao X, Shimoji K, Marnett LJ, Johnson CR, and Honn KV (1994). Endogenous 12(*S*)-HETE production by tumor cells and its role in metastasis. *Cancer Res* **54,** 1574–1579.

[7] Nie D, Hillman GG, Geddes T, Tang K, Pierson C, Grignon DJ, and Honn KV (1998). Platelet-type 12-lipoxygenase in a human prostate carcinoma stimulates angiogenesis and tumor growth. *Cancer Res* **58,** 4047–4051.

[8] Ghosh J and Myers CE (1998). Inhibition of arachidonate 5-lipoxygenase triggers massive apoptosis in human prostate cancer cells. *Proc Natl Acad Sci USA* **95,** 13182–13187.

[9] Kelavkar U, Hutzley J, Dhir R, Kim P, Allen K, and McHugh K (2006). Prostate tumor growth and recurrence can be modulated by the omega (ω)-6: ω-3 ratio in diet: athymic mouse xenograft model simulating radical prostatectomy. *Neoplasia* **8,** 112–124.

[10] Kelavkar U, Cohen C, Eling T, and Badr K (2002). 15-Lipoxygenase-1 overexpression in prostate adenocarcinoma. *Adv Exp Med Biol* **507,** 133–145.

[11] Kelavkar UP, Nixon JB, Cohen C, Dillehay D, Eling TE, and Badr KF (2001). Overexpression of 15-lipoxygenase-1 in PC-3 human prostate cancer cells increases tumorigenesis. *Carcinogenesis* **22,** 1765–1773.

[12] Kelavkar UP and Cohen C (2004). 15-Lipoxygenase-1 expression upregulates and activates insulin-like growth factor-1 receptor in prostate cancer cells. *Neoplasia* **6,** 41–52.

[13] Reddy N, Everhart A, Eling T, and Glasgow W (1997). Characterization of a 15-lipoxygenase in human breast carcinoma BT-20 cells: stimulation of 13-HODE formation by TGF alpha/EGF. *Biochem Biophys Res Commun* **231,** 111–116.

[14] Bertomeu MC, Gallo S, Lauri D, Haas TA, Orr FW, Bastida E, and Buchanan MR (1993). Interleukin 1–induced cancer cell/endothelial cell adhesion *in vitro* and its relationship to metastasis *in vivo*: role of vessel wall 13-HODE synthesis and integrin expression. *Clin Exp Metastasis* **11,** 243–250.

[15] Buchanan MR, Horsewood P, and Brister SJ (1998). Regulation of endothelial cell and platelet receptor–ligand binding by the 12- and 15-lipoxygenase monohydroxides, 12-, 15-HETE and 13-HODE. *Prostaglandins Leukot Essent Fat Acids* **58,** 339–346.

[16] Natarajan R and Nadler J (1998). Role of lipoxygenases in breast cancer. *Front Biosci* **3,** E81–E88.

[17] Cesano A, Visonneau S, Scimeca JA, Kritchevsky D, and Santoli D (1998). Opposite effects of linoleic acid and conjugated linoleic acid on human prostatic cancer in SCID mice. *Anticancer Res* **18,** 1429–1434.

[18] Zock PL and Katan MB (1998). Linoleic acid intake and cancer risk: a review and meta-analysis. *Am J Clin Nutr* **68,** 142–153.

[19] Kamitani H, Geller M, and Eling T (1998). Expression of 15-lipoxygenase by human colorectal carcinoma Caco-2 cells during apoptosis and cell differentiation. *J Biol Chem* **273,** 21569–21577.

[20] Kelavkar U, Glasgow W, and Eling TE (2002). The effect of 15-lipoxygenase-1 expression on cancer cells. *Curr Urol Rep* **3,** 207–214.

[21] Glasgow WC, Afshari CA, Barrett JC, and Eling TE (1992). Modulation of the epidermal growth factor mitogenic response by metabolites of linoleic and arachidonic acid in Syrian hamster embryo fibroblasts. Differential effects in tumor suppressor gene (+) and (−) phenotypes. *J Biol Chem* **267,** 10771–10779.

[22] Sauer LA, Dauchy RT, Blask DE, Armstrong BJ, and Scalici S (1999). 13-Hydroxyoctadecadienoic acid is the mitogenic signal for linoleic acid–dependent growth in rat hepatoma 7288CTC *in vivo*. *Cancer Res* **59,** 4688–4692.

[23] Blask DE, Sauer LA, Dauchy RT, Holowachuk EW, Ruhoff MS, and Kopff HS (1999). Melatonin inhibition of cancer growth *in vivo* involves suppression of tumor fatty acid metabolism *via* melatonin receptor–mediated signal transduction events. *Cancer Res* **59,** 4693–4701.

[24] Blask DE, Dauchy RT, Sauer LA, and Krause JA (2004). Melatonin uptake and growth prevention in rat hepatoma 7288CTC in response to dietary melatonin: melatonin receptor–mediated inhibition of tumor linoleic acid metabolism to the growth signaling molecule 13-hydroxyoctadecadienoic acid and the potential role of phytomelatonin. *Carcinogenesis* **25,** 951–960.

[25] Kelavkar UP and Badr KF (1999). Effects of mutant *p53* expression on human 15-lipoxygenase-promoter activity and murine 12/15-lipoxygenase gene expression: evidence that 15-lipoxygenase is a mutator gene. *Proc Natl Acad Sci USA* **96,** 4378–4383.

[26] Coleman K, Kelavkar U, Lawson D, Haseman J, and Cohen C (2002). 15-Lipoxygenase-1 (15-LO-1) as a molecular marker in cancer: an immunohistochemical study. *Mod Pathol* **15,** 304A.

[27] Kelavkar UP, Harya N, Hutzley J, Bacich DJ, Monzon FA, Chandran U, Dhir R, and O'Keefe DS (2006). DNA methylation paradigm shift: 15-lipoxygenase-1 upregulation in prostatic intraepithelial neoplasia and prostate cancer by atypical promoter hypermethylation. *Prostaglandins and Other Lipid Mediat* (in press).

[28] Shureiqi I, Wojno KJ, Poore JA, Reddy RG, Moussalli MJ, Spindler SA, Greenson JK, Normolle D, Hasan AA, Lawrence TS, et al. (1999). Decreased 13-*S*-hydroxyoctadecadienoic acid levels and 15-lipoxygenase-1 expression in human colon cancers. *Carcinogenesis* **20,** 1985–1995.

[29] Shureiqi I, Wu Y, Chen D, Yang XL, Guan B, Morris JS, Yang P, Newman RA, Broaddus R, Hamilton SR, et al. (2005). The critical role of 15-lipoxygenase-1 in colorectal epithelial cell terminal differentiation and tumorigenesis. *Cancer Res* **65,** 11486–11492.

[30] Shureiqi I, Xu X, Chen D, Lotan R, Morris JS, Fischer SM, and Lippman SM (2001). Nonsteroidal anti-inflammatory drugs induce apoptosis in esophageal cancer cells by restoring 15-lipoxygenase-1 expression. *Cancer Res* **61,** 4879–4884.

[31] Hanson JA, Gillespie JW, Grover A, Tangrea MA, Chuaqui RF, Emmert-Buck MR, Tangrea JA, Libutti SK, Linehan WM, and Woodson KG (2006). Gene promoter methylation in prostate tumor-associated stromal cells. *J Natl Cancer Inst* **98,** 255–261.

[32] Shappell SB, Thomas GV, Roberts RL, Herbert R, Ittmann MM, Rubin MA, Humphrey PA, Sundberg JP, Rozengurt N, Barrios R, et al. (2004).

Prostate pathology of genetically engineered mice: definitions and classification. The consensus report from the Bar Harbor meeting of the Mouse Models of Human Cancer Consortium Prostate Pathology Committee. *Cancer Res* **64,** 2270–2305.

[33] Jackson EL, Willis N, Mercer K, Bronson RT, Crowley D, Montoya R, Jacks T, and Tuveson DA (2001). Analysis of lung tumor initiation and progression using conditional expression of oncogenic K-ras. *Genes Dev* **15,** 3243–3248.

[34] Wu X, Wu J, Huang J, Powell WC, Zhang J, Matusik RJ, Sangiorgi FO, Maxson RE, Sucov HM, and Roy-Burman P (2001). Generation of a prostate epithelial cell–specific Cre transgenic mouse model for tissue-specific gene ablation. *Mech Dev* **101,** 61–69.

[35] Araki K, Araki M, Miyazaki J, and Vassalli P (1995). Site-specific recombination of a transgene in fertilized eggs by transient expression of Cre recombinase. *PNAS* **92,** 160–164.

[36] Hogan B (1994). In: Manipulating the Mouse Embryo: A Laboratory Manual, 2nd ed. Cold Spring Harbor Press, Woodbury, NY.

[37] Pothier F, Ouellet M, Julien JP, and Guerin SL (1992). An improved CAT assay for promoter analysis in either transgenic mice or tissue culture cells. *DNA Cell Biol* **11,** 83–90.

[38] Folkvord JM, Viders D, Coleman-Smith A, and Clark RA (1989). Optimization of immunohistochemical techniques to detect extracellular matrix proteins in fixed skin specimens. *J Histochem Cytochem* **37,** 105–113.

[39] Sheehan DC and Hrapchak BB (1980). Theory and Practice of Histotechnology. C. V. Mosby Co., St. Louis.

[40] Kelavkar UP, Glasgow W, Olson SJ, Foster BA, and Shappell SB (2004). Overexpression of 12/15-lipoxygenase, an ortholog of human 15-lipoxygenase-1, in the prostate tumors of TRAMP mice. *Neoplasia* **6,** 821–830.

[41] Kasper S (2005). Survey of genetically engineered mouse models for prostate cancer: analyzing the molecular basis of prostate cancer development, progression, and metastasis. *J Cell Biochem* **94,** 279–297.

[42] Wechter WJ, Leipold DD, Murray ED Jr, Quiggle D, McCracken JD, Barrios RS, and Greenberg NM (2000). E-7869 (R-flurbiprofen) inhibits progression of prostate cancer in the TRAMP mouse. *Cancer Res* **60,** 2203–2208.

[43] Kaplan PJ, Mohan S, Cohen P, Foster BA, and Greenberg NM (1999). The insulin-like growth factor axis and prostate cancer: lessons from the transgenic adenocarcinoma of mouse prostate (TRAMP) model. *Cancer Res* **59,** 2203–2209.

[44] Ruijter E, van de Kaa C, Miller G, Ruiter D, Debruyne F, and Schalken J (1999). Molecular genetics and epidemiology of prostate carcinoma. *Endocr Rev* **20,** 22–45.

[45] Sporn MB and Suh N (2002). Chemoprevention: an essential approach to controlling cancer. *Nat Rev Cancer* **2,** 537–543.

[46] Nelson WG, DeWeese TL, and DeMarzo AM (2002). The diet, prostate inflammation, and the development of prostate cancer. *Cancer Metastasis Rev* **21,** 3–16.

[47] Nelson WG, De Marzo AM, Deweese TL, Lin X, Brooks JD, Putzi MJ, Nelson CP, Groopman JD, and Kensler TW (2001). Preneoplastic prostate lesions: an opportunity for prostate cancer prevention. *Ann NY Acad Sci* **952,** 135–144.

[48] Henrique R, Jeronimo C, Teixeira MR, Hoque MO, Carvalho AL, Pais I, Ribeiro FR, Oliveira J, Lopes C, and Sidransky D (2006). Epigenetic heterogeneity of high-grade prostatic intraepithelial neoplasia: clues for clonal progression in prostate carcinogenesis. *Mol Cancer Res*, 1541–7786 (MCR-05-0113).

[49] Shappell SB, Olson SJ, Hannah SE, Manning S, Roberts RL, Masumori N, Jisaka M, Boeglin WE, Vader V, Dave DS, et al. (2003). Elevated expression of 12/15-lipoxygenase and cyclooxygenase-2 in a transgenic mouse model of prostate carcinoma. *Cancer Res* **63,** 2256–2267.

[50] Abate-Shen C, Banach-Petrosky WA, Sun X, Economides KD, Desai N, Gregg JP, Borowsky AD, Cardiff RD, and Shen MM (2003). Nkx3.1; *Pten* mutant mice develop invasive prostate adenocarcinoma and lymph node metastases. *Cancer Res* **63,** 3886–3890.

[51] Abdulkadir SA, Magee JA, Peters TJ, Kaleem Z, Naughton CK, Humphrey PA, and Milbrandt J (2002). Conditional loss of Nkx3.1 in adult mice induces prostatic intraepithelial neoplasia. *Mol Cell Biol* **22,** 1495–1503.

[52] Kim MJ, Bhatia-Gaur R, Banach-Petrosky WA, Desai N, Wang Y, Hayward SW, Cunha GR, Cardiff RD, Shen MM, and Abate-Shen C (2002). *Nkx3.1* mutant mice recapitulate early stages of prostate carcinogenesis. *Cancer Res* **62,** 2999–3004.

[53] Kim MJ, Cardiff RD, Desai N, Banach-Petrosky WA, Parsons R, Shen MM, and Abate-Shen C (2002). Cooperativity of Nkx3.1 and Pten loss of function in a mouse model of prostate carcinogenesis. *Proc Natl Acad Sci USA* **99,** 2884–2889.

[54] Shen MM and Abate-Shen C (2003). Roles of the *Nkx3.1* homeobox gene in prostate organogenesis and carcinogenesis. *Dev Dyn* **228,** 767–778.

[55] Dunn JE (1975). Cancer epidemiology in populations of the United States—with emphasis on Hawaii and California—and Japan. *Cancer Res* **35,** 3240–3245.

[56] Yang YJ, Lee SH, Hong SJ, and Chung BC (1999). Comparison of fatty acid profiles in the serum of patients with prostate cancer and benign prostatic hyperplasia. *Clin Biochem* **32,** 405–409.

[57] Freeman VL, Meydani M, Yong S, Pyle J, Flanigan RC, Waters WB, and Wojcik EM (2000). Prostatic levels of fatty acids and the histopathology of localized prostate cancer. *J Urol* **164,** 2168–2172.

[58] Yegnasubramanian S, Kowalski J, Gonzalgo ML, Zahurak M, Piantadosi S, Walsh PC, Bova GS, De Marzo AM, Isaacs WB, and Nelson WG (2004). Hypermethylation of CpG islands in primary and metastatic human prostate cancer. *Cancer Res* **64,** 1975–1986.

[59] Abate-Shen C and Shen MM (2000). Molecular genetics of prostate cancer. *Genes Dev* **14,** 2410–2434.

[60] Abate-Shen C and Shen MM (2002). Mouse models of prostate carcinogenesis. *Trends Genet* **18,** S1–S5.

[61] Huss WJ, Maddison LA, and Greenberg NM (2001). Autochthonous mouse models for prostate cancer: past, present and future. *Semin Cancer Biol* **11,** 245–260.

[62] Powell WC, Cardiff RD, Cohen MB, Miller GJ, and Roy-Burman P (2003). Mouse strains for prostate tumorigenesis based on genes altered in human prostate cancer. *Curr Drug Targets* **4,** 263–279.

[63] Raghow S, Hooshdaran MZ, Katiyar S, and Steiner MS (2002). Toremifene prevents prostate cancer in the transgenic adenocarcinoma of mouse prostate model. *Cancer Res* **62,** 1370–1376.

[64] Raghow S, Kuliyev E, Steakley M, Greenberg N, and Steiner MS (2000). Efficacious chemoprevention of primary prostate cancer by flutamide in an autochthonous transgenic model. *Cancer Res* **60,** 4093–4097.

[65] Mentor-Marcel R, Lamartiniere CA, Eltoum IE, Greenberg NM, and Elgavish A (2001). Genistein in the diet reduces the incidence of poorly differentiated prostatic adenocarcinoma in transgenic mice (TRAMP). *Cancer Res* **61,** 6777–6782.

[66] Backman SA, Ghazarian D, So K, Sanchez O, Wagner KU, Hennighausen L, Suzuki A, Tsao MS, Chapman WB, Stambolic V, et al. (2004). Early onset of neoplasia in the prostate and skin of mice with tissue-specific deletion of Pten. *Proc Natl Acad Sci USA* **101,** 1725–1730.

[67] Di Cristofano A, De Acetis M, Koff A, Cordon-Cardo C, and Pandolfi PP (2001). Pten and p27KIP1 cooperate in prostate cancer tumor suppression in the mouse. *Nat Genet* **27,** 222–224.

[68] Di Cristofano A, Pesce B, Cordon-Cardo C, and Pandolfi PP (1998). Pten is essential for embryonic development and tumour suppression. *Nat Genet* **19,** 348–355.

[69] Podsypanina K, Ellenson LH, Nemes A, Gu J, Tamura M, Yamada KM, Cordon-Cardo C, Catoretti G, Fisher PE, and Parsons R (1999). Mutation of Pten/Mmac1 in mice causes neoplasia in multiple organ systems. *Proc Natl Acad Sci USA* **96,** 1563–1568.

[70] Wang W, Bergh A, and Damber JE (2005). Cyclooxygenase-2 expression correlates with local chronic inflammation and tumor neovascularization in human prostate cancer. *Clin Cancer Res* **11,** 3250–3256.